

RECONCILING OPTICAL AND RADIO OBSERVATIONS OF THE BINARY MILLISECOND PULSAR PSR J1640+2224

SARAH J. VIGELAND¹, ADAM T. DELLER², DAVID L. KAPLAN¹, ALINA G. ISTRATE¹, BENJAMIN W. STAPPERS³, THOMAS M. TAURIS^{4,5}

Draft version March 20, 2018

ABSTRACT

Previous optical and radio observations of the binary millisecond pulsar PSR J1640+2224 have come to inconsistent conclusions about the identity of its companion, with some observations suggesting the companion is a low-mass helium-core (He-core) white dwarf (WD), while others indicate it is most likely a high-mass carbon-oxygen (CO) WD. Binary evolution models predict PSR J1640+2224 most likely formed in a low-mass X-ray binary (LMXB) based on the pulsar’s short spin period and long-period, low-eccentricity orbit, in which case its companion should be a He-core WD with mass about $0.35 - 0.39 M_{\odot}$, depending on metallicity. If it is instead a CO WD, that would suggest the system has an unusual formation history. In this paper we present the first astrometric parallax measurement for this system from observations made with the Very Long Baseline Array (VLBA), from which we determine the distance to be 1520^{+170}_{-150} pc. We use this distance and a reanalysis of archival optical observations originally taken in 1995 with the Wide Field Planetary Camera 2 (WFPC2) on the *Hubble Space Telescope* (*HST*) in order to measure the WD’s mass. We also incorporate improvements in calibration, extinction model, and WD cooling models. We find that the existing observations are not sufficient to tightly constrain the companion mass, but we conclude the WD mass is $> 0.4 M_{\odot}$ with $> 90\%$ confidence. The limiting factor in our analysis is the low signal-to-noise ratio of the original *HST* observations.

1. INTRODUCTION

Millisecond pulsars (MSPs) are valuable laboratories for studying a wide range of physics and astrophysics topics, including binary evolution (Champion et al. 2008), neutron star formation (Demorest et al. 2010; Özel & Freire 2016; Tauris et al. 2017), the equation of state of nuclear matter (Lattimer 2011), and gravitation (Antoniadis et al. 2013). MSPs can also be used to observe low-frequency gravitational waves (GWs) as part of pulsar timing arrays (Hellings & Downs 1983; Lentati et al. 2015; Shannon et al. 2015; Arzoumanian et al. 2016). These experiments rely on pulsar timing, whereby the times of arrival (TOAs) of pulses are fit to a complex timing model that incorporates the astrometric, spin, and binary properties of the pulsar (Edwards et al. 2006). For some MSPs, other radio and optical observations can provide independent measurements of some of these parameters, which can be used to verify and improve pulsar timing solutions.

PSR J1640+2224 is a fully-recycled MSP with spin period $P = 3.16$ ms. It is in a wide, nearly circular binary (orbital period $P_b = 175$ days, orbital eccentricity $e = 7.9725 \times 10^{-4}$) with a white dwarf (WD) compan-

ion (Lundgren et al. 1996b). Pulsar timing observations have been able to detect the Shapiro delay—a relativistic time delay caused by the pulses’ propagation through the companion’s gravitational potential— from which the companion’s mass can be measured (Shapiro 1964). However, drawing conclusions from those data has been complicated by the fact that the orbital period is very close to half a year, resulting in degeneracies between some of the binary and astrometric parameters. Initial work by Löhmer et al. (2005) reported a low companion mass of $M_c = 0.15^{+0.08}_{-0.05} M_{\odot}$. Subsequent timing campaigns have not been able to reproduce consistent results. Demorest et al. (2013) reported a companion mass of $M_c = 0.25 \pm 0.04 M_{\odot}$ based on five years of observations taken as part of the North American Nanohertz Observatory for Gravitational Waves (NANOGrav). However, an analysis of the same data by Vigeland & Vallisneri (2014) using Bayesian inference to perform the timing fit found a 95% probability that the companion mass is above $0.3 M_{\odot}$. Most recently, Fonseca et al. (2016) presented an even higher value of $M_c = 0.6^{+0.4}_{-0.2} M_{\odot}$ based on nine years of observations.

In addition, while optical observations of WDs can determine their masses and effective temperatures, in this case the constraints are very weak. Based on observations with the Palomar 200-in. telescope, Lundgren et al. (1996a) concluded $T_{\text{eff}} = 3700 \pm 300$ K and $M_c < 0.47 M_{\odot}$. An analysis of observations made with the Wide Field Planetary Camera 2 (WFPC2) on the *Hubble Space Telescope* (*HST*) by Lundgren et al. (1996b) found $T_{\text{eff}} = 4200 \pm 300$ K and $M_c = 0.25 \pm 0.10 M_{\odot}$, but a later analysis of the same data by Hansen & Phinney (1998) yielded $T_{\text{eff}} = 4460 \pm 1125$ K and an allowed mass range of $0.25 - 0.45 M_{\odot}$. Both of these analyses were limited by

¹ University of Wisconsin-Milwaukee, P.O. Box 413, Milwaukee, WI 53201 USA

² Centre for Astrophysics and Supercomputing, Swinburne University of Technology, PO Box 218, Hawthorn, VIC 3122, Australia

³ Jodrell Bank Centre for Astrophysics, School of Physics and Astronomy, The University of Manchester, Manchester M13 9PL, UK

⁴ Max-Planck-Institut für Radioastronomie, Auf dem Hügel 69, D-53121 Bonn, Germany

⁵ Argelander-Institut für Astronomie, Universität Bonn, Auf dem Hügel 71, 53121 Bonn, Germany

the large uncertainty in the pulsar distance, which was estimated from the observed pulse-dispersion properties measure and the Taylor & Cordes (1993) model of the Galactic electron density distribution.

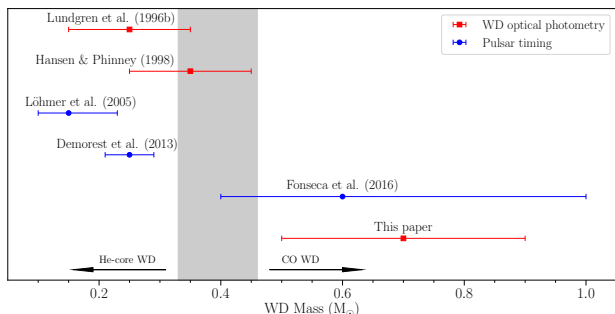


FIG. 1.— Published masses for the WD companion of PSR J1640+2224. We show the median values and 68%-confidence intervals. The red squares indicate values obtained from optical photometry of the WD, and the blue circles indicate values obtained from pulsar timing. The shaded region between $0.33 M_{\odot}$ and $0.46 M_{\odot}$ shows the mass cutoff between He-core and CO WDs.

The large range in the reported companion masses (see Fig. 1) has important implications for binary evolution models. The small pulsar spin period and wide, nearly circular orbit point to this system forming from a wide-orbit low-mass X-ray binary (LMXB; Tauris 2011). Models of LMXBs predict a correlation between the orbital period and WD mass, which for this system implies the companion mass is $0.35 - 0.39 M_{\odot}$ depending on the metallicity (Rappaport et al. 1995; Tauris & Savonijje 1999; van Kerkwijk et al. 2005; Istrate et al. 2016; see Fig. 2). If the companion is significantly more massive, as suggested by some results from pulsar timing, then how the system formed is uncertain. Most pulsars with massive WD companions formed in intermediate-mass X-ray binaries (IMXBs; Tauris 2011). However, PSR J1640+2224 has a smaller spin period, longer orbital period, and smaller orbital eccentricity than most binary pulsars formed this way. In particular, the combination of these characteristics makes it difficult to understand the formation of PSR J1640+2224 if it has a CO WD companion and thus formed from an IMXB.

In this paper, we present the first astrometric parallax measurement for PSR J1640+2224 based on observations taken with the Very Long Baseline Array (VLBA). We use this distance to reanalyze the 1995 *HST* observations of PSR J1640+2224. We also improve upon the original analysis by taking advantage of improved photometry software, updated calibration of WFPC2 (Dolphin 2000, 2009), a new 3D map of Galactic extinction (Green et al. 2015), and updated WD cooling models (Tremblay et al. 2011; Bergeron et al. 2011). Our analysis of two other pulsars observed in the same manner, PSR J1022+1001 and PSR J2145-0750, were published in Deller et al. (2016).

This paper is organized as follows. In Sec. 2 we describe the very long baseline interferometry (VLBI) observations used to measure the astrometric parallax and transverse velocity of the system. In Sec. 3 we describe the optical observations and data reduction techniques

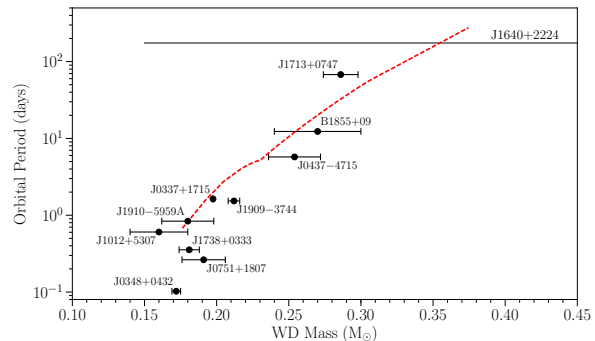


FIG. 2.— Orbital period and WD mass for binary MSPs with He-core WD companions. The red dashed line shows the theoretical $P_{\text{orb}} - M_c$ relationship, assuming a metallicity of $Z = 0.02$ (Istrate et al. 2016). The circles represent the measured orbital periods and WD masses, with their uncertainties, for about a dozen binary MSPs. All of the measured WD masses are in good agreement with the theoretical relationship. The gray horizontal line represents the published median values for the WD companion mass of PSR J1640+2224, which range from $0.15 M_{\odot}$ (Löhmer et al. 2005) to $0.6 M_{\odot}$ (Fonseca et al. 2016). Figure modified from Swiggum et al. (2017).

used. In Sec. 4 we discuss the procedure used to fit the photometry data to the WD cooling curves to obtain the temperature and mass of the WD. We summarize our findings in Sec. 5.

2. VLBI OBSERVATIONS

We observed PSR J1640+2224 a total of 11 times with the VLBA in the period 2015 August to 2017 August under the project codes BD179 and BD192, as part of the MSPSR π project⁶. The observing and data reduction strategy are similar to that used previously in Deller et al. (2016) for PSRs J1022+1001 and J2145-0750 and described in detail in the PSR π catalog paper (Deller et al., in prep). PSR J1640+2224 is one of the first sources in the MSPSR π program to complete observations; results for a total of 18 millisecond pulsars (including a comparison of VLBI-derived to timing-derived positions and proper motions to test frame alignment) will be available over the coming 12 months.

The VLBA's maximum recording rate of 2 gigabits per second was employed to sample 256 MHz of bandwidth in dual polarization at each antenna, spanning the range 1392.0–1744.0 MHz while avoiding regions contaminated by radio frequency interference. The source J1594+1029 was observed once per observation to calibrate the instrumental delays and bandpass, while J1641+2257 was observed every 5 minutes to calibrate atmospheric/ionospheric delays and phases. Around 40 minutes on the target source PSR J1640+2224 was obtained per observation.

To refine the atmospheric/ionospheric phase calibration in the pulsar direction and produce the highest quality astrometry, the use of a secondary phase calibrator (preferably in the same field of view as the target pulsar) is highly desirable. A total of four suitably compact and bright background sources were identified in the same field as PSR J1640+2224 during a short exploratory observation prior to the commencement of astrometry in

⁶ <https://safe.nrao.edu/vlba/psrpi/status.html>

TABLE 1
VLBI CALIBRATOR SOURCES

Source	Right Ascension	Declination	Reference
J1641+2257	16:41:25.227564	22:57:04.03284	RFC2015a ^a
J163919.7+221120	16:39:19.77745	22:11:20.0485	This work
J164018.7+222917	16:40:18.71436	22:29:17.4158	This work
J164018.9+221203	16:40:18.90807	22:12:03.9182	This work
J164044.3+221016	16:40:44.38302	22:10:16.4713	This work

^a<http://astrogeo.org/rfc/>

2015, in which the multi-field capability of the DiFX correlator used at the VLBA (Deller et al. 2011) was employed to inspect every known radio source with 30' of PSR J1640+2224. The source J164018.9+221203 was the brightest source in the field (flux density ~ 100 mJy, angular separation 12' from PSR J1640+2224) and was used for secondary phase calibration, while the other sources are used for consistency checks. The positions used for all relevant calibrator sources are shown in Table 1; the in-beam source reference positions are derived from relative astrometry to J1641+2257 (reference epoch MJD 57500), using the observations presented here.

For each astrometric observation, a total of six correlated datasets were produced: one for each of the background sources, and two at the position of PSR J1640+2224, where one correlation employed pulsar gating (Deller et al. 2007) to boost sensitivity on the pulsar, and one was ungated. The pulsar gating made use of an ephemeris derived from observations with the Lovell telescope and was used for all astrometry, while the ungated dataset was used to check the correctness of the pulsar ephemeris. Calibration was derived and applied in the manner described in Deller et al. (2016), and used a solution interval of 6 seconds for secondary phase calibration (frequency independent) and 90 seconds for secondary phase calibration (frequency dependent). A position time series for each of the five in-beam sources (4 background and the pulsar) was obtained via imaging and position fitting as described in Deller et al. (2016). Finally, we add an additional component in quadrature to the position uncertainties at each epoch based on the angular separation between the source and the secondary phase calibrator J164018.9+221203, to account for systematic position errors resulting from the differential ionosphere. The component added in quadrature ranged from 0.05 – 0.2 mas depending on the source, and was calculated using empirical results from the PSR π VLBI astrometric campaign containing 60 pulsars (Deller et al. 2016, Deller et al. in prep).

We fit each position time series for reference position, proper motion, and parallax using the linear least-squares solver `pmpar`⁷. For PSR J1640+2224, we performed fits using the affine-invariant Markov chain Monte Carlo (MCMC) ensemble sampler `emcee` (Foreman-Mackey et al. 2013), solving additionally for orbital inclination i and longitude of ascending node Ω in order to account for orbital reflex motion. We used uniform priors for all parameters, excluding only values $i \leq 14^\circ$, which are ruled out by the mass function obtained by pulsar timing for a companion mass $\leq 1.4 M_\odot$, assuming the pulsar mass is $\geq 1.2 M_\odot$. We also cross-checked

⁷ <https://github.com/walterfb/pmpar>

TABLE 2
VLBI ASTROMETRIC PARAMETER FITS

Parameter	Value
R.A. (J2000)	16:40:16.74587 \pm 0.00007
Decl. (J2000)	22:24:08.764 \pm 0.001
Position epoch (MJD)	57500
R.A. offset ^A (mas)	-29985.23 \pm 0.07
Decl. offset ^A (mas)	724845.93 \pm 0.12
μ_α (mas yr ⁻¹)	2.19 \pm 0.08
μ_δ (mas yr ⁻¹)	-11.28 \pm 0.14
Parallax (mas)	0.66 \pm 0.07
Distance (pc)	1520 ⁺¹⁷⁰ ₋₁₅₀
v_T (km s ⁻¹)	82 ⁺¹¹ ₋₉

^A Relative to the reference position for J164018.9+221203.

our results using bootstrap sampling in the manner described in Deller et al. (2016), obtaining consistent values and uncertainties. The results (with 68% credible intervals) are shown in Table 2 and plotted in Figure 3. No significant constraints could be placed on i or Ω based on the orbital reflex motion, which was small compared to the typical position uncertainty in a single epoch. The unknown reflex motion did, however, lead to larger uncertainties on the parallax and proper motion, and so if the inclination in particular could be better constrained, the distance and transverse velocity uncertainties for PSR J1640+2224 could be further reduced. The VLBI-estimated position and proper motion are consistent at the 1- σ level with the 9-year NANOGrav results presented by Matthews et al. (2016).

As an additional cross-check, we inspected the astrometric fits for the three other background sources not used for secondary phase calibration. In the absence of calibration errors, if all sources are distant background objects that do not exhibit structural variations, then their fitted proper motions and parallaxes should be consistent with zero. In most cases, the fitted values are consistent with zero, and in almost all cases they are smaller than the uncertainties on the corresponding parameters for PSR J1640+2224. The exceptions were J163919.7+221120, with a significant measurement of $\mu_\alpha = 0.17 \pm 0.05$ mas yr⁻¹, and J164018.7+222917 with $\mu_\alpha = 0.26 \pm 0.12$ mas yr⁻¹. Both of these sources have a larger angular separation to the secondary phase calibrator than does PSR J1640+2224, meaning that any systematic errors in the fitted parameters for PSR J1640+2224 should be smaller than these values. If structural evolution in J163919.7+221120 or J164018.7+222917 played a significant role in producing these offsets, then the maximum expected value of any systematic errors for PSR J1640+2224 would be even smaller.

3. OPTICAL OBSERVATIONS

PSR J1640+2224 was observed with the Wide Field and Planetary Camera 2 (WFPC2) aboard *HST* in October 1995 as part of a program to observe WD companions of six MSPs. The source was imaged with the Planetary Camera (PC) detector. Images were made with the F555W (*V*-band) and F814W (*I*-band) filters with exposure times of 1000 s and 800 s, respectively. Figure 4 shows a drizzled (Fruchter & Hook 2002) combined image downloaded from the Hubble Legacy Archive. The

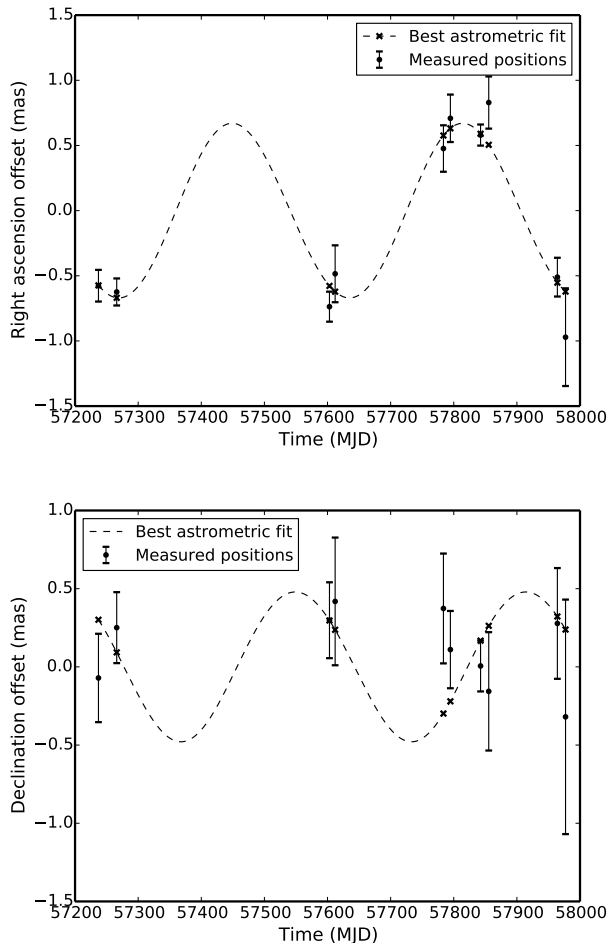


FIG. 3.— Relative position offset for PSR J1640+2224 in right ascension (top) and declination (bottom) as a function of time, after subtracting proper motion to highlight the parallax contribution. For plotting purposes, the poorly constrained orbital reflex motion has been neglected.

absolute astrometry has been improved to $0''.3$, compared to $0''.8$ from Lundgren et al. (1996b).

Data reduction was done with *HSTphot* (version 1.1; Dolphin 2000). We masked bad pixels, estimated the sky level, and masked cosmic rays by comparing exposure pairs. We used point-spread function (PSF) fitting photometry using the revised calibration of Dolphin (2009). Since the fields were relatively sparse, we did not allow *HSTphot* to determine the PSF residual and we used the default aperture corrections. There were no significant differences in the final magnitudes when we varied the processing steps. We found 25.52 ± 0.12 mag in the F555W filter, and 24.62 ± 0.16 mag in the F814W filter. Our F814W magnitude is the same as the value reported by Lundgren et al. (1996b), but our F555W magnitude is 0.5 mag brighter (a 1.7-sigma difference).

The extinction and its uncertainty were obtained from the 3D Galactic dust map by Green et al. (2015), which gives the reddening $E(B - V)$ along the line of sight as a function of distance, using the VLBI-measured distance. We converted from $E(B - V)$ to the extinctions in each band using $R_V = 3.1$ and the extinction coefficients A_λ

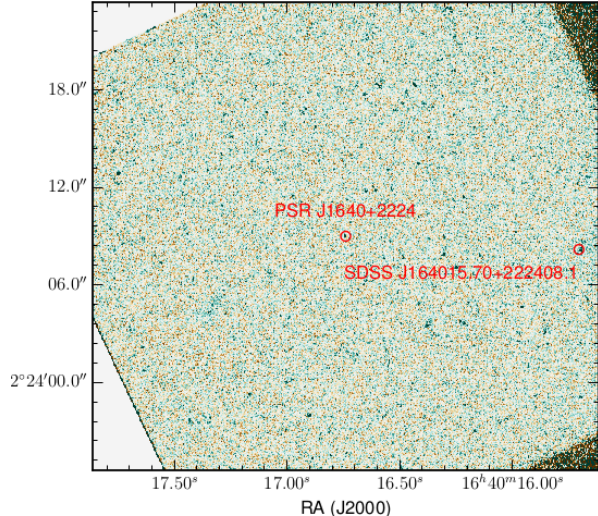


FIG. 4.— Drizzled (Fruchter & Hook 2002) image of PSR J1640+2224 from *HST* observations by Lundgren et al. (1996b) using WFPC2. The central red circle indicates the position of the pulsar based on pulsar timing observations, corrected to the observation epoch. The circle’s radius of $0''.3$ reflects the absolute astrometric uncertainty. The optical source, located inside the red circle, is consistent with the pulsar. For reference, the other red circle indicates a source from the Sloan Digital Sky Survey (Ahn et al. 2014). The astrometric agreement allows us to conclude that we have in fact identified the counterpart to PSR J1640+2224 (cf. Lundgren et al. 1996b).

from Girardi et al. (2008), with an additional 15% reduction in A_λ based on the revised calibration in Schlafly & Finkbeiner (2011), and found $A_V = 0.12 \pm 0.03$.

4. WD ATMOSPHERE FITTING

We fit the photometry using both hydrogen-atmosphere (DA) and helium-atmosphere (DB) models from Tremblay et al. (2011) and Bergeron et al. (2011), respectively⁸. These models tabulate synthetic photometry integrated throughout the *HST*/WFPC2 filter passbands in the Vega system (like *hstphot*) for a range of effective temperatures, masses, and radii. To simplify our analysis, we only used WD atmosphere models for a single reference mass M_{ref} . We compared the model magnitudes with the observed apparent magnitudes according to

$$m = M + 5 \log_{10} \left(\frac{d}{10 \text{ pc}} \right) + A_\lambda - 5 \log_{10} \left[\frac{R_c(T_{\text{eff}}, M_c)}{R_{\text{ref}}} \right],$$

where m is the observed apparent magnitude, M is the absolute magnitude from the WD models, d is the distance, A_λ is the extinction in a particular band, R_c is the WD radius, T_{eff} is the effective temperature, and M_c is the WD mass. R_{ref} is the radius of a WD with temperature T_{eff} and whose mass is the reference mass M_{ref} . The final term in this expression incorporates the dependence on the WD mass and radius by adjusting the magnitudes based on the ratio between the WD radius for a particular effective temperature and WD mass $[R_c(T_{\text{eff}}, M_c)]$ and the radius for that temperature and the model mass $[R_{\text{ref}}]$. This simplification introduces an

⁸ Also see <http://www.astro.umontreal.ca/~bergeron/CoolingModels/>.

TABLE 3
WD PARAMETER FITS

Parameter	DA WD	DB WD
T_{eff} (K)	6090^{+780}_{-590}	6000^{+790}_{-570}
d (pc)	1520^{+180}_{-140}	1520^{+170}_{-140}
A_V	$0.12^{+0.03}_{-0.03}$	$0.12^{+0.03}_{-0.03}$
R_c ($10^{-2}R_{\odot}$)	$1.12^{+0.26}_{-0.23}$	$1.18^{+0.24}_{-0.26}$
M_c (M_{\odot})	$0.71^{+0.21}_{-0.20}$	$0.66^{+0.21}_{-0.19}$
χ^2	1.33	1.54

NOTE. — Values are the median and 68% confidence intervals from the marginalized posterior distributions.

error of < 0.1 mag, which is smaller than the photometric uncertainties.

We used two sets of models to determine the WD radius. Since the DA and DB models assume a carbon-oxygen (CO) core, we only used the WD radius from these models for $M_c \geq 0.4 M_{\odot}$, where the assumption of a CO core is likely correct. For $M_c < 0.4 M_{\odot}$, we used low-mass He-core WD models from Istrate et al. (2016) to determine the radius as a function of mass and temperature.

We performed the model fits with the affine-invariant Markov chain Monte Carlo (MCMC) ensemble sampler `emcee` (Foreman-Mackey et al. 2013). We used a uniform prior on T_{eff} between 4000 and 10000 K, and a Gaussian prior on A_{λ} with mean and standard deviation determined from the Green et al. (2015) 3D Galactic dust map for this distance and line of sight. We used a Gaussian prior on the parallax centered around the VLBI-measured value and a uniform prior on the WD mass between 0.2 and $1.2 M_{\odot}$.

Table 3 lists the best-fit values, and Fig. 5 shows the posterior distributions obtained using DA and DB WD models. We find an effective temperature of $T_{\text{eff}} = 6090^{+780}_{-590}$ K and $T_{\text{eff}} = 6000^{+790}_{-570}$ K for DA and DB WDs, respectively. These values are significantly higher than the value reported by Lundgren et al. (1996b), but they are consistent with those in Hansen & Phinney (1998). For the WD mass, we find $M_c = 0.71^{+0.21}_{-0.20} M_{\odot}$ with DA models and $M_c = 0.66^{+0.21}_{-0.19} M_{\odot}$ with DB models, and our results indicate $M_c > 0.4 M_{\odot}$ with $> 90\%$ -confidence for both DA and DB models. This suggests the companion is most likely a CO WD.

5. DISCUSSION AND CONCLUSIONS

Here we present measurements of the parallax and transverse velocity of PSR J1640+2224 from VLBI astrometry, including the first precise distance measurement for this system. We measured an annual geometric parallax of 0.66 ± 0.07 mas, which yields a distance of 1520^{+170}_{-150} pc. We used this distance measurement to re-analyze the 1995 *HST* observations of PSR J1640+2224 in order to infer the WD companion’s mass. We were also able to improve upon the original analysis by taking advantage of improvements in *HST* calibration, updated WD cooling models, and a new 3D model of Galactic dust.

The original analysis by Lundgren et al. (1996b) identified the companion as a low-mass He-core WD with $T_{\text{eff}} = 4200 \pm 300$ K and $M_c = 0.25 \pm 0.10 M_{\odot}$. Our

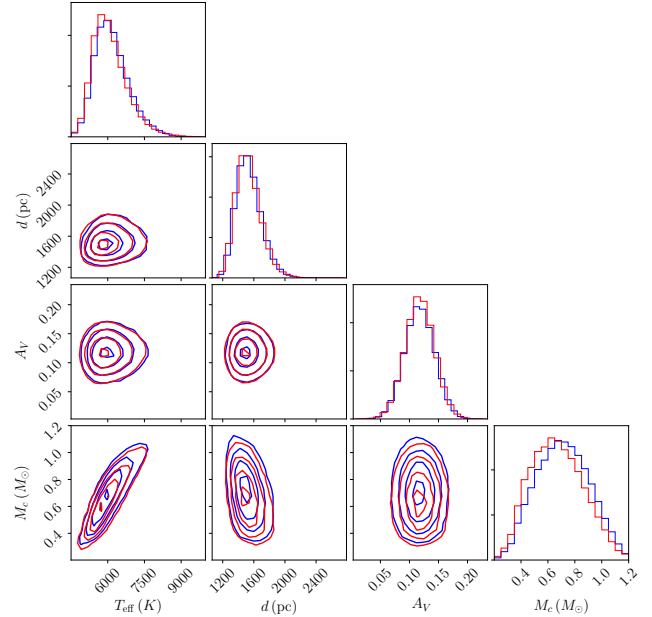


FIG. 5.— Joint two-dimensional posterior probability distributions and marginalized one-dimensional posterior probability distributions from fitting the *HST* photometry to WD cooling models. We use the VLBI-measured parallax as a prior on the distance, and a Gaussian prior on the extinction A_V with mean and standard deviation taken from the Green et al. (2015) 3D galactic dust map. We show fits to both DA model WDs (blue curves) and DB model WDs (red curves). Best-fit parameter values and uncertainties are listed in Table 3.

reanalysis found a significantly higher temperature of $T_{\text{eff}} = 6090^{+780}_{-590}$ K and $T_{\text{eff}} = 6000^{+790}_{-570}$ K for DA and DB WDs, respectively. We also found a higher companion mass than previously reported, $M_c = 0.71^{+0.21}_{-0.20} M_{\odot}$ with DA models and $M_c = 0.66^{+0.21}_{-0.19} M_{\odot}$ with DB models. Our analysis finds $M_c > 0.4 M_{\odot}$ with $> 90\%$ -confidence for both DA and DB models, indicating the companion is mostly likely a CO WD, rather than a He-core WD as formation models predict.

Identifying the WD companion as either a He-core WD or CO WD has implications for NS-WD binary formation models. The low spin period indicates PSR J1640+2224 has been fully recycled, and that combined with its low orbital eccentricity implies it formed in a LMXB, in which case its companion should be a He-core WD. If that is the case, a precise measurement of the WD mass can be used to constrain the theoretical $P_b - M_c$ relationship for wide-orbit LMXBs. There are only a dozen observations known to verify this relationship since relatively few pulsar binaries have precise measurements of the companion mass, especially in wide systems with $P_b > 20$ days (Tauris & van den Heuvel 2014). Furthermore, there are a number of factors that may affect the WD mass, including the convective mixing-length parameter and the metallicity of the WD progenitor star (Tauris & Savonije 1999; Stairs et al. 2005; Shao & Li 2012; Istrate et al. 2016).

If the companion is instead a CO WD, then the formation of this system is a puzzle. Most pulsars with CO WD companions formed in IMXBs, which typically yield partially-recycled MSPs with relatively long

spin periods ($P > 10$ ms) and short orbital periods ($P_b < 40$ days). However, there are exceptions. The binary pulsar J1614–2230 has a massive CO WD companion and a spin period of 3.15 ms, which is comparable to PSR J1640+2224, although its orbital period is significantly shorter ($P_b = 8$ days; Tauris et al. 2011, 2012). Another possibility is that PSR J1640+2224’s formation involved dynamical encounters, as is believed to be the case for PSR J1903+0327 (Champion et al. 2008), PSR J1835–3259A (DeCesar et al. 2015), and PSR J1024–0719 (Kaplan et al. 2016; Bassa et al. 2016). However, PSR J1903+0327 and PSR J1835–3259A both have highly eccentric orbits⁹ whereas PSR J1640+2224 is in a nearly circular orbit.

Measurements of the WD mass are limited by the low S/N of the original observations, as well as having observations in only two filters (V -band and I -band). Higher precision optical observations in three or more filters could be used to get a more precise mass measurement. Additionally, long-term high-cadence timing observations of PSR J1640+2224 may be able to break the degeneracies in the timing model between the astromet-

ric and binary parameters, allowing for the companion mass to be measured via the Shapiro delay.

We thank Saul Rappaport and Joris Verbiest for helpful comments and suggestions. SJV and DLK are funded by the NSF Physics Frontiers Center award number 1430284. AGI acknowledges support from the NASA Astrophysics Theory Program through NASA grant NNX13AH43G. Access to the Lovell Telescope and pulsar research at the Jodrell Bank Centre for Astrophysics is supported through an STFC consolidated grant. The Long Baseline Observatory is a facility of the National Science Foundation operated under cooperative agreement by Associated Universities, Inc. Based on observations made with the NASA/ESA *Hubble Space Telescope*, and obtained from the Hubble Legacy Archive, which is a collaboration between the Space Telescope Science Institute (STScI/NASA), the Space Telescope European Coordinating Facility (ST-ECF/ESA) and the Canadian Astronomy Data Centre (CADC/NRC/CSA).
Facilities: HST (WFPC2), VLBA

REFERENCES

- Ahn, C. P., Alexandroff, R., Allende Prieto, C., et al. 2014, *ApJS*, 211, 17
- Antoniadis, J., Freire, P. C. C., Wex, N., et al. 2013, *Science*, 340, 448
- Arzoumanian, Z., Brazier, A., Burke-Spolaor, S., et al. 2016, *ApJ*, 821, 13
- Bassa, C. G., Janssen, G. H., Stappers, B. W., et al. 2016, *MNRAS*, 460, 2207
- Bergeron, P., Wesemael, F., Dufour, P., et al. 2011, *ApJ*, 737, 28
- Champion, D. J., Ransom, S. M., Lazarus, P., et al. 2008, *Science*, 320, 1309
- DeCesar, M. E., Ransom, S. M., Kaplan, D. L., Ray, P. S., & Geller, A. M. 2015, *ApJ*, 807, L23
- Deller, A. T., Tingay, S. J., Bailes, M., & West, C. 2007, *PASP*, 119, 318
- Deller, A. T., Brisken, W. F., Phillips, C. J., et al. 2011, *PASP*, 123, 275
- Deller, A. T., Vigeland, S. J., Kaplan, D. L., et al. 2016, *ApJ*, 828, 8
- Demorest, P. B., Pennucci, T., Ransom, S. M., Roberts, M. S. E., & Hessels, J. W. T. 2010, *Nature*, 467, 1081
- Demorest, P. B., Ferdman, R. D., Gonzalez, M. E., et al. 2013, *ApJ*, 762, 94
- Dolphin, A. E. 2000, *PASP*, 112, 1383
- . 2009, *PASP*, 121, 655
- Edwards, R. T., Hobbs, G. B., & Manchester, R. N. 2006, *MNRAS*, 372, 1549
- Fonseca, E., Pennucci, T. T., Ellis, J. A., et al. 2016, *ApJ*, 832, 167
- Foreman-Mackey, D., Hogg, D. W., Lang, D., & Goodman, J. 2013, *PASP*, 125, 306
- Fruchter, A. S., & Hook, R. N. 2002, *PASP*, 114, 144
- Girardi, L., Dalcanton, J., Williams, B., et al. 2008, *PASP*, 120, 583
- Green, G. M., Schafly, E. F., Finkbeiner, D. P., et al. 2015, *ApJ*, 810, 25
- Hansen, B. M. S., & Phinney, E. S. 1998, *MNRAS*, 294, 569
- Hellings, R. W., & Downs, G. S. 1983, *ApJ*, 265, L39
- Istrate, A. G., Marchant, P., Tauris, T. M., et al. 2016, *A&A*, 595, A35
- Kaplan, D. L., Kupfer, T., Nice, D. J., et al. 2016, *ApJ*, 826, 86
- Lattimer, J. M. 2011, *Ap&SS*, 336, 67
- Lentati, L., Taylor, S. R., Mingarelli, C. M. F., et al. 2015, *MNRAS*, 453, 2576
- Löhmer, O., Lewandowski, W., Wolszczan, A., & Wielebinski, R. 2005, *ApJ*, 621, 388
- Lundgren, S. C., Cordes, J. M., Foster, R. S., Wolszczan, A., & Camilo, F. 1996a, *ApJ*, 458, L33
- Lundgren, S. C., Foster, R. S., & Camilo, F. 1996b, in *Astronomical Society of the Pacific Conference Series*, Vol. 105, IAU Colloq. 160: Pulsars: Problems and Progress, ed. S. Johnston, M. A. Walker, & M. Bailes, 497
- Matthews, A. M., Nice, D. J., Fonseca, E., et al. 2016, *ApJ*, 818, 92
- Ozel, F., & Freire, P. 2016, arXiv:1603.02698, arXiv:1603.02698
- Rappaport, S., Podsiadlowski, P., Joss, P. C., Di Stefano, R., & Han, Z. 1995, *MNRAS*, 273, 731
- Schafly, E. F., & Finkbeiner, D. P. 2011, *ApJ*, 737, 103
- Shannon, R. M., Ravi, V., Lentati, L. T., et al. 2015, *Science*, 349, 1522
- Shao, Y., & Li, X.-D. 2012, *ApJ*, 756, 85
- Shapiro, I. I. 1964, *Physical Review Letters*, 13, 789
- Stairs, I. H., Faulkner, A. J., Lyne, A. G., et al. 2005, *ApJ*, 632, 1060
- Swiggum, J. K., Kaplan, D. L., McLaughlin, M. A., et al. 2017, *ApJ*, 847, 25
- Tauris, T. M. 2011, in *Astronomical Society of the Pacific Conference Series*, Vol. 447, *Evolution of Compact Binaries*, ed. L. Schmidtobreick, M. R. Schreiber, & C. Tappert, 285
- Tauris, T. M., Langer, N., & Kramer, M. 2011, *MNRAS*, 416, 2130
- . 2012, *MNRAS*, 425, 1601
- Tauris, T. M., & Savonije, G. J. 1999, *A&A*, 350, 928
- Tauris, T. M., & van den Heuvel, E. P. J. 2014, *ApJ*, 781, L13
- Tauris, T. M., Kramer, M., Freire, P. C. C., et al. 2017, *ApJ*, 846, 170
- Taylor, J. H., & Cordes, J. M. 1993, *ApJ*, 411, 674
- Tremblay, P.-E., Bergeron, P., & Gianninas, A. 2011, *ApJ*, 730, 128
- van Kerkwijk, M. H., Bassa, C. G., Jacoby, B. A., & Jonker, P. G. 2005, in *Astronomical Society of the Pacific Conference Series*, Vol. 328, *Binary Radio Pulsars*, ed. F. A. Rasio & I. H. Stairs, 357
- Vigeland, S. J., & Vallisneri, M. 2014, *MNRAS*, 440, 1446

⁹ The orbital eccentricity of PSR J1024–0719 is not well con-

strained due to the extremely long orbital period.